Journal of Alloys and Compounds 488 (2009) 148–156

Contents lists available at ScienceDirect

Journal of Alloys and Compounds

journal homepage: www.elsevier.com/locate/jallcom

Review

FPLAPW study of the structural, electronic, and optical properties of Ga_2O_3: Monoclinic and hexagonal phases

F. Litimein [a], D. Rached [a,*], R. Khenata [b], H. Baltache [b]

[a] Laboratoire des Matériaux Magnétiques, Département de Physique, Faculté des Sciences, Université Djillali Liabes de Sidi Bel Abbès, Sidi Bel Abbès - 22000, Algeria
[b] Laboratoire de Physique Quantique et de Modélisation Mathématique de la Matière (LPQ3M), Centre Universitaire de Mascara, Mascara - 29000, Algeria

ARTICLE INFO

Article history:
Received 30 April 2009
Received in revised form 9 August 2009
Accepted 14 August 2009
Available online 27 August 2009

PACS:
71.20.Nr
78.20.Ci
81.05.Je
71.15.Ap
71.15.Mb

Keywords:
FPLAPW
Electronic properties
Optical properties
High pressure

ABSTRACT

Using the first principles full-potential linearized augmented plane-wave method within the local density approximation, we have studied the structural, electronic and optical properties of Ga_2O_3 in its ambient, monoclinic (β) and high-pressure hexagonal (α) phases. It is found the both β-Ga_2O_3 and α-Ga_2O_3 have an indirect band gap. The conduction band minimum (CBM) is located at Γ point for both phases, whereas the valence band maximum (VBM) is located at the M point for β-Ga_2O_3 and at L point for α-Ga_2O_3. The calculated total and partial density of states are also presented. The analysis of the electron charge density shows that the Ga–O bonds have significant ionic character. The anisotropic optical properties are investigated by means of the complex dielectric function, which are explained by the selection rule of the band-to-band transitions. For the monoclinic phase, it is shown that the component with y-direction are more pronounced than that along the x and z.

Contents

1. Introduction

Gallium oxide (Ga_2O_3) can adopt five different crystalline structures depending upon the conditions of preparation, that is, α, β, γ, δ and ε phases [1–3]. Among these phases, β-Ga_2O_3 is an important wide band gap compound which has good thermal and chemical stability [3,4]. It has drawn significant attention from scientists because of its potential application in different fields as luminescent material [5,6], including flat panel displays, solar energy conversion devices, optical limiters for deep ultraviolet radiation [5,7,8], high temperature stable gas sensors [9,10], antireflection coating on GaAs [11,12], passivation coating [13], etc. It can also be used as a transparent conducting oxide of optoelectronic devices [13–15]. Besides, the magnetism of the conduction electron spin of β-Ga_2O_3 exhibits an original memory effect with a wide range of temperatures from 4 K to room temperature [16]. On the order hand, syntheses of 1-dimensional gallium oxide structures like nanorods, -belts, and -wires [17,18] have been also reported.

* Corresponding author.
E-mail addresses: flitimein@yahoo.fr (F. Litimein), rachdj@yahoo.fr (D. Rached).

0925-8388/$ – see front matter © 2009 Elsevier B.V. All rights reserved.
doi:10.1016/j.jallcom.2009.08.092

At ambient condition, the structure of β-Ga_2O_3 is monoclinic. It has a melting point of 1725 °C and is obtained by calcination of hydroxide, nitrate, acetate or oxalate at temperature above 600 °C. It is observed to undergo a first-order phase transition to the hexagonal α-Ga_2O_3 phase at 4.4 GPa at 1000 °C. This one can be obtained by heating gallium oxide hydroxide (or 'gallic diaspore'), GaO(OH), at 300–500 °C, or by heating β-gallium(III) oxide at 6.5 kbar and 1100 °C for 1 h. Recently, using synchrotron X-ray diffraction and Raman spectroscopy in diamond anvil cells Machon et al. [19] studied the high-pressure behavior of Ga_2O_3 up to 40 GPa. However, it has been shown in different reports [2,3,20] that nanostructure of α-Ga_2O_3 is easily obtained at relatively low temperature, and its conversion to the β form requires a temperature >500 °C, sometimes with an intermediate temperature range where phases coexist, $\alpha \rightarrow \alpha + \beta \rightarrow \beta$ [3,20]. Unfortunately, may be it being a major phase, properties of α-Ga_2O_3 thin films are less not reported.

On the theoretical side, there are relatively fewer theoretical studies [21–26] on Ga_2O_3 specially in its α phase, in spite of the availability of numerous experimental studies [6,7,11,27–39]. The electronic structure and optical properties of β-Ga_2O_3 has been calculated by Kenji Yamaguchi using the full-potential linearized augmented plane wave (FPLAPW) [23]. Yoshioka et al. [26] investigated the structural properties of five Ga_2O_3 polymorphs, using the pseudopotential method combined with GGA functional. The structural, electronic and optical properties of this compound in its monoclinic and hexagonal phases have been discussed by He et al. [25], using the linear combination of atomic orbital (LCAO) method within the Becke's three-parameter hybrid exchange functional (B3LYP).

In this paper we focus on the structural, electronic, and optical properties of Ga_2O_3 in its ambient and high-pressure phases, using the experimental coordinates as given in Refs. [40,41], respectively. To the best of our knowledge, no full potential calculations on these properties have been reported yet. Hence, we addressed ourselves to perform these calculations by using another accurate full-potential linear augmented plane-wave plus local orbital (FP-LAPW + lo) method in order to provide a comparative and a complementary study for these properties. The rest of the paper is organized as follows. In Section 2, we outline the theoretical framework within which all the calculations have been performed. In Section 3, we present and discuss the results of our study concerning the structural properties Section 3.1, the electronic properties Section 3.2, and the optical properties Section 3.3 of β-Ga_2O_3 and α-Ga_2O_3 systems. Finally, in Section 4 we summarize our conclusions.

2. Details of calculations

The equilibrium structural parameters were calculated using the Vienna package WIEN2K [42]. This is an implementation of a hybrid full-potential (linear) augmented plane-wave plus local orbitals (L/APW + lo) method within the density-functional theory [43,44]. This new approach is shown to reproduce the accurate results of the LAPW method, but using a smaller basis set size. Due to the smaller basis set and faster matrix set up, APW + lo offers a shorter run-time and uses less memory than LAPW. The effects of using APW + lo are greatest for calculations with a large ratio of basis functions to atoms, e.g. for open crystal structures, surfaces and molecules on surfaces [45].

The APW + lo method expands the Kohn–Sham orbitals in atomic like orbitals inside the atomic muffin-tin (MT) spheres and plane waves in the interstitial region. The details of the method have been described in the literature [45–47]. The basis set inside each MT sphere is split into core and valence subsets. The core states are treated within the spherical part of the potential only and are assumed to have a spherically symmetric charge density totally confined inside the MT spheres. The valence part is treated within a potential expanded into spherical harmonics up to $l = 4$. The valence wave functions inside the spheres are expanded up to $l = 10$. A plane-wave expansion with $R_{MT} \times K_{MAX}$ equal to 8. The k-points mesh in the full Brillouin zone turns out to be satisfactory with a k sampling $5 \times 5 \times 5$ and $4 \times 4 \times 4$ for both β and α phase, respectively. All of the calculations were carried out at the theoretical equilibrium lattice constants.

We take the Perdew–Wang local density approximation (LDA) [48]. The self-consistent calculations are considered to be converged only when the calculated total energy of the crystal

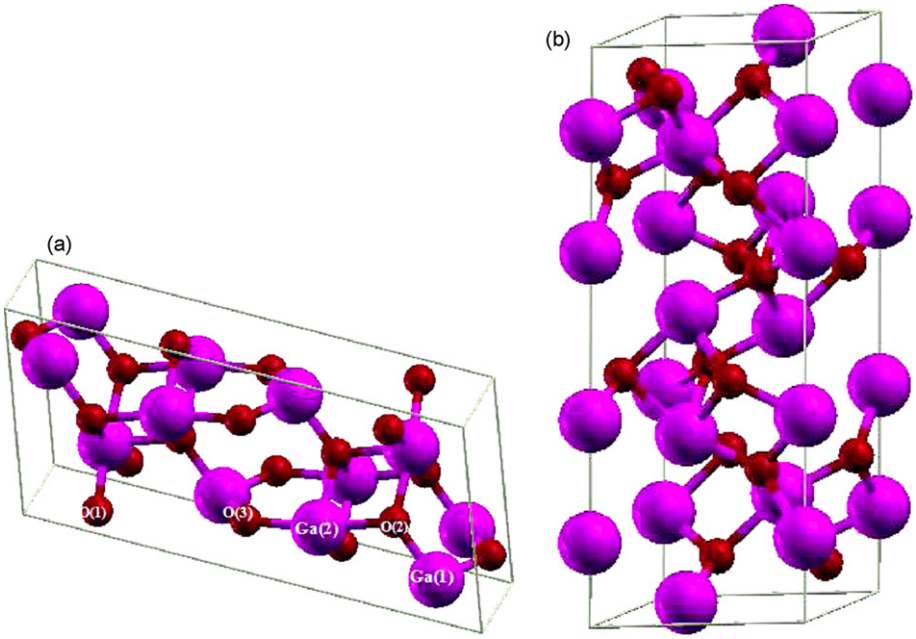

Fig. 1. Schematic illustration of crystalline structures of (a) β-Ga_2O_3 (the three oxygen sites with different symmetry are denoted by O(1), O(2), and O(3). Gallium atoms are in tetrahedral or octahedral coordination, denoted by Ga(1) and Ga(2), respectively) and (b) α-Ga_2O_3.

Table 1
Calculated bulk properties at zero-pressure of β and α phases of Ga_2O_3. Experimentals and theoreticals values are included for comparison.

Phase	Property	Present	B3LYP-DFT[a]	GGA[b]	GGA[c]	Expt.
β	a (Å)	12.208	12.34	12.438	12.27	12.23[d]
	b (Å)	3.031	3.08	3.084	3.03	3.04[d]
	c (Å)	5.751	5.87	5.877	5.80	5.80
	β (°)	103.63	103.9	103.71	103.7	103.7
	B (Mbar)	218.57	174		330	
	B'	3.153	3.79		1.7	
α	a (Å)	4.952	5.04	5.059		4.983[e]
	c (Å)	13.319	13.56	13.618		13.433[e]
	B (Mbar)	243.659	210			
	B'	3.813	4.95			

[a] Ref. [25].
[b] Ref. [26].
[c] Ref. [24].
[d] Ref. [40].
[e] Ref. [41].

converged to less than 1 mRyd. The choice of the particular (and different) muffin-tin (MT) radii for gallium and oxygen atoms shows small differences that does not affect our results. We compute lattice constants and bulk moduli by fitting the total energy versus volume according to the Murnaghan's equation of state [49].

3. Results and discussion

3.1. Structural properties

The unit cell of the monoclinic phase (Fig. 1(a)) has $C2/m$ symmetry, in which there are two crystallographically nonequivalent Ga atoms and three nonequivalent O atoms, all of them located at $4i$ (x, 0, z) [40].

The hexagonal phase or Corundum structure α-Ga_2O_3 (Fig. 1(b)) is rhombohedral, with $R\bar{3}c$ space group in which the cations lay in $12c$ (0, 0, z) Wyckhoff positions and the oxygen atoms in $18e$ (x, 0, 1/4) Wyckhoff positions [41].

To obtain the equilibrium lattice parameters, we have used the experimental crystal coordinates given in references [40,41] for both structure β and α, respectively and varied the lattice parameters a, b, c and the angle β independently while computing the energy. The lowest-energy configuration resulted in the parameters given in Table 1 which were close to the experimental data [40,41]. The calculated unit cell volume was 2.5% and 2.0% less than the experimental value for β and α phases, respectively which is common for DFT calculations using the LDA exchange-correlation functional. Otherwise, it is clearly seen that the α structure has the highest bulk modulus value. Therefore, we can expect that this phase should exhibit higher hardness than β, assuming that the hardness scales with the bulk modulus.

The optimized atomic positions are given in Table 2 and they were not only in agreement with the experimental positions [40,41] but also with the values reported by He et al. [25] which are also given for comparison.

Ga_2O_3 compound thermodynamically stable in the $C2/m$ phase tends to undergo a $R\bar{3}c$ phase transition when increasing the pressure. To find out the transition pressure, Gibbs free energy relation $G = E + PV - TS$ is applied. Being the phase transition pressure independent of the temperature, last term is ignored, and corresponding relation for Gibbs free energy reduces to enthalpy relation $H = E + PV$.

At a given pressure a stable structure is one for which enthalpy has its lowest value and the transition pressures are calculated at which the enthalpies for the phases are equal. In Fig. 2, we plot the energy of Gibbs in which we consider the β phase like a reference. We determine the phase transition pressure to be 9.28 GPa, associated with a volume for the β phase of 46.93 Å^3 and for the α phase of 51.42 Å^3. Our results tends to support the calculated value of the transition pressure 9.5 GPa of Ref. [25], and the experimental value 4.4 GPa of Ref. [50].

3.2. Electronic properties

For both phases, the electronic band structures have been calculated at the equilibrium lattice. The most prominent features of the calculated band structures (band gaps and bandwidths) are shown in Table 3. It is interestingly noted that β-Ga_2O_3 has indirect band gap with the valence-band maximum (VBM) at M and the conduction-band minimum (CBM) at Γ, while α-Ga_2O_3 has indirect band gap with the VBM at L and the CBM at Γ. The energy at Γ being 0.026 eV lower than that at M for β phase, and 0.12 eV lower than that at L for α phase. The results of our calculations within LDA approximation are in fairly good agreement with LCAO-DFT

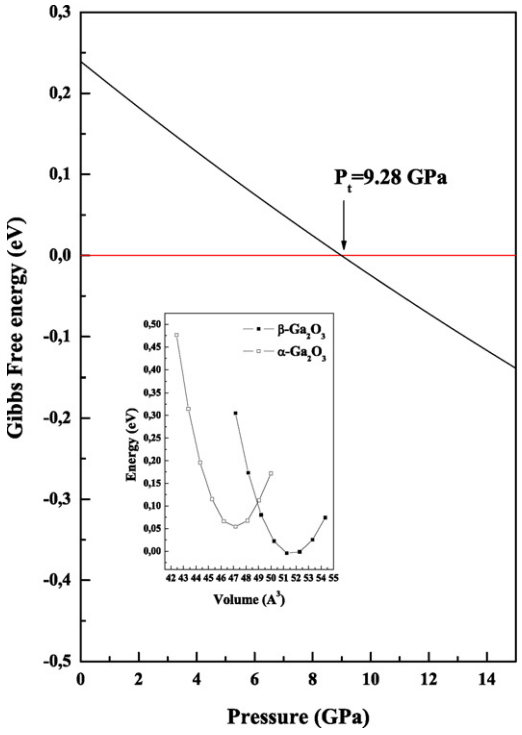

Fig. 2. Gibbs free energies per formula unit at temperature $T = 0$ of β and α phases of Ga_2O_3. Small inset is the energy vs. volume per formula unit of β and α phases of Ga_2O_3. The reference energy in set for the β phase.

Table 2
The unit cell contents of β-Ga_2O_3 and α-Ga_2O_3 given in fractional coordinates. Experimentals and theoreticals values are included for comparison.

β-Ga_2O_3				α-Ga_2O_3			
Property	Present	B3LYP-DFT[a]	Expt.[b]	Property	Present	B3LYP-DFT[a]	Expt.[c]
Fractional coordinates				Fractional coordinates			
x_{Ga_1}	0.091	0.091	0.090	z_{Ga}	0.355	0.356	0.3554
z_{Ga_1}	0.795	0.794	0.795	x_O	0.303	0.302	0.3049
x_{Ga_2}	0.341	0.342	0.341				
z_{Ga_2}	0.685	0.686	0.686				
x_{O_1}	0.166	0.163	0.167				
z_{O_1}	0.109	0.109	0.101				
x_{O_2}	0.496	0.495	0.496				
z_{O_2}	0.253	0.257	0.255				
x_{O_3}	0.827	0.826	0.828				
z_{O_3}	0.439	0.436	0.436				

[a] Ref. [25].
[b] Ref. [40].
[c] Ref. [41].

calculations [25] for the valence and conduction band configurations. We would like to note that the experimental values of the band gap of Ga_2O_3 lie in the range from 4.23 to 4.99 eV for thin films [6,11,27–29,33,39], and from 4.6 to 5.1 eV for single crystals [4,7].

In Figs. 3 and 4, we show the calculations of the total and the partial DOSs for both β- and α-Ga_2O_3. At around −19 to −17 eV, there are 6 bands mainly composed of O 2s states. At around −13 to −11.5 eV, there are 20 bands mainly composed of Ga 3d states. The upper part of the valence bands is mainly formed by the O 2p states with a width of about 7.25 and 7.3 eV for β and α phases, respectively. The bottom of the conduction band consists mainly of the Ga 4s states. For β-Ga_2O_3, there are more localized charges around the octahedral Ga(2) site compared with Ga(1) for the CBM. For the VBM, on the other hand, nearly 50% of the charges are located at the O(1) site, and the remainder is mostly distributed at the other oxygen sites and in the interstitial region.

Figs. 5(a) and 6(a) shows the calculated total charge density of β- and α-Ga_2O_3 in the plane parallel to the *b*-axis containing the Ga–O bonds. We have also presented the density difference distributions to analyze bonding in the crystal. A definition of ionic and covalent binding based on density difference distributions is presented in Figs. 5(b) and 6(b). It has been pointed out before that some covalent bonding character between Ga and O may exist [24]. The ionic or covalent character in β- and α-Ga_2O_3 is a somewhat controversial topic and has important bearings on the proper interpretation of transport data in these materials. For the monoclinic structure, this covalency can be clearly seen in the bonds Ga(1)–O(2) due to its lower coordination in the crystalline lattice. Indeed, the nuclei are bound by the density which is shared between them. For the other atoms and in the hexagonal phase (see Figs. 5(b) and 6(b)), the electrons are localized in basins around the O atoms, and there is no bond localization region, suggesting a mainly ionic bonding (i.e. the density is localized on a single nucleus).

3.3. Optical properties

A deeper understanding of electronic structures can be obtained by studying optical spectra which not only give information about the occupied and unoccupied states, but also about the character of bands. Therefore we have calculated the optical properties for the β- and α-Ga_2O_3 structure and compared them with available

Table 3
Calculated LDA band gaps (in eV), upper-valence bandwidth UVB (in eV), and total-valence bandwidth TVB (in eV) for the β-Ga_2O_3 and α-Ga_2O_3 compared to other theoretical calculations. Values of the experimental gaps are also shown.

Phase	Property	Present	B3LYP-DFT, Ref. [25]	GGA, Ref. [24]	GGA, Ref. [26]	Expt.
β	Γ–Γ (eV)	2.388	4.69	4.40		4.60[a], 4.66[b], 4.9[c]
	Γ–Γ (eV)	2.362	4.66	4.37	1.8	
	Γ–Z (eV)	4.558	2.37	6.61		
	Γ–A (eV)	4.721	2.65	6.99		
	Γ–M (eV)	5.145	2.83	7.11		
	Γ–V (eV)	5.351	3.59	7.69		
	Γ–L (eV)	6.617	5.23	9.42		
	UVB	7.25	7.01	7.00		
	TVB	18.83				
α	Γ–Γ (eV)	3.295	5.08			4.7[d], 4.9[e], 4.98[f], 4.99[g]
	L–Γ (eV)	3.172	5.03		2.4	
	F–Γ (eV)	3.181	5.03			
	Γ–Z (eV)	6.286	3.25			
	Γ–L (eV)	6.774	3.68			
	Γ–F (eV)	6.988	3.83			
	UVB	7.3	7.10			
	TVB	19.12				

[a] Ref. [4].
[b] Ref. [7]. The measured values represent an average of the anisotropic ones along the *c*-axis (4.79 eV) and *b*-axis (4.52 eV).
[c] Ref. [33].
[d] Ref. [55].
[e] Ref. [54].
[f] Ref. [20].
[g] Ref. [39].

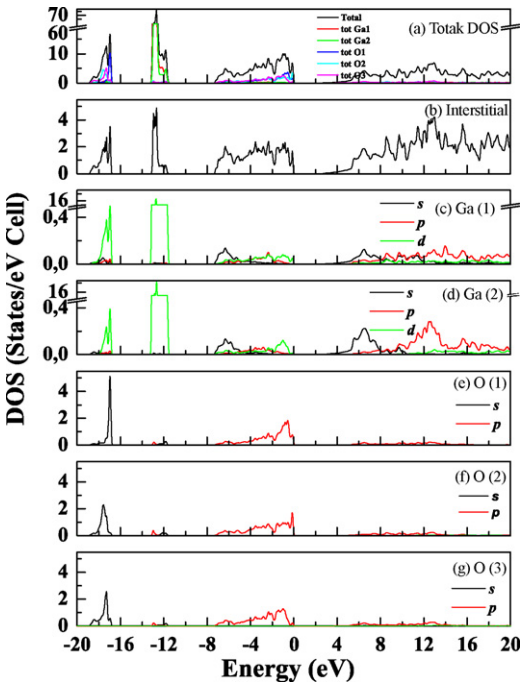

Fig. 3. (a–g) Total and projected density of states of β-Ga_2O_3. The Fermi energy is aligned to zero.

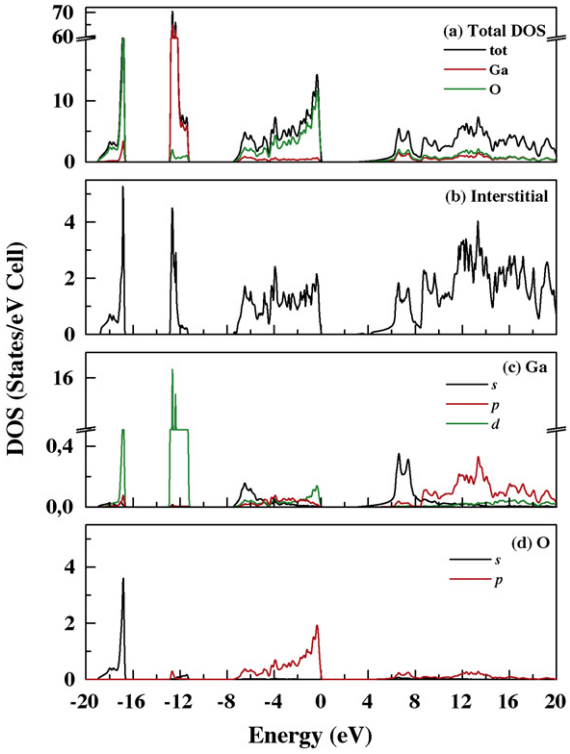

Fig. 4. (a–d) Total and projected density of states of α-Ga_2O_3. The Fermi energy is aligned to zero.

experimental data. Once energies ε_{ck} and functions $|\mathbf{k}\rangle$ for the n bands are obtained self-consistently, the interband contribution to the imaginary part of the dielectric functions $\varepsilon_2(\omega)$ can be calculated by summing transitions from occupied to unoccupied states with fixed k vector over the BZ, weighted with the appropriate matrix element for the probability of the transition.

From the band structure, we can calculate the imaginary part $\varepsilon_2(\omega)$ of the dielectric function as a function of photon energy. Here we use also the experimental value of band gap and consider the band gap correction (ΔE_g) to be 2.238 and 1.628 eV for both β and α phases, respectively, which shifts the onset of calculated $\varepsilon_2(\omega)$ upwards in photon energy. After band gap correction, the real part of the dielectric function $\varepsilon_1(\omega)$ can be derived from $\varepsilon_2(\omega)$ according to Kramers–Kronig dispersion relationship.

Figs. 7 and 8, display the calculated real $\varepsilon_1(\omega)$ and imaginary $\varepsilon_2(\omega)$ parts of the dielectric function for a radiation up to 50 eV, where the black line is calculated results, the red line is the calculated results from He et al. In the figure, we can see that our calculated results are consistent with the results of He and co-workers obtained from periodic linear combination of atomic orbitals (LCAO) method for both phases and to those of Yamaguchi by using the FPLAPW for the β phase. There are a number of critical points exhibited in the calculated imaginary part of the dielectric function.

For the monoclinic phase, the absorption edges of the polarized dipoles along the x- and z-directions starts at about 2.36 and

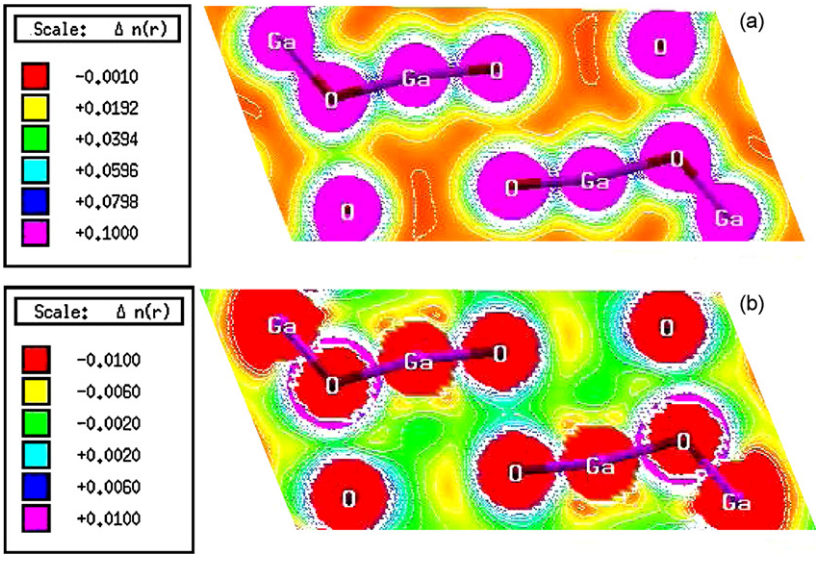

Fig. 5. Contour map of (a) total charge density (b) difference charge density on the (0 1 0) plane of β-Ga_2O_3.

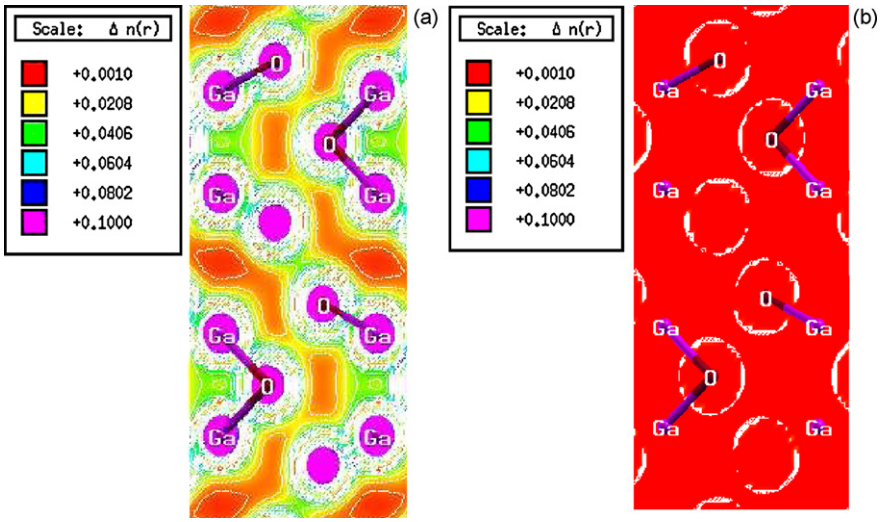

Fig. 6. Contour map of (a) total charge density (b) difference charge density on the (0 1 0) plane of α-Ga_2O_3.

2.52 eV which are related to the minimum band gap corresponding to the direct transition Γ–Γ. On the other hand, an about 0.76 eV larger absorption edge is found for the polarized dipole along the *y*-direction which starts at about 3.12 eV. Such gap represent the transition between the 52nd and 57th levels at the Γ point. The energy shift between the 52nd and 56th levels is 0.74 eV, which coincides with the shift of the anisotropic absorption edge in Fig. 8 (see in parallel Table 4). The difference in the anisotropy between the *y* component and *x*/*z* component can be related to the chain-type structure along the *b*-axis. For the hexagonal phase, the dispersion along *x*/*y* component can be distinguished from that along *z*. However, the absorption start at about 3.2 eV along *x*/*y*-directions and 3.3 eV along *z* direction which is related to the transition between 57 and 56 bands and 57–55 bands at point Γ, respectively.

Through the calculated electronic band structures and density of states, we can explain the different peak structures seen

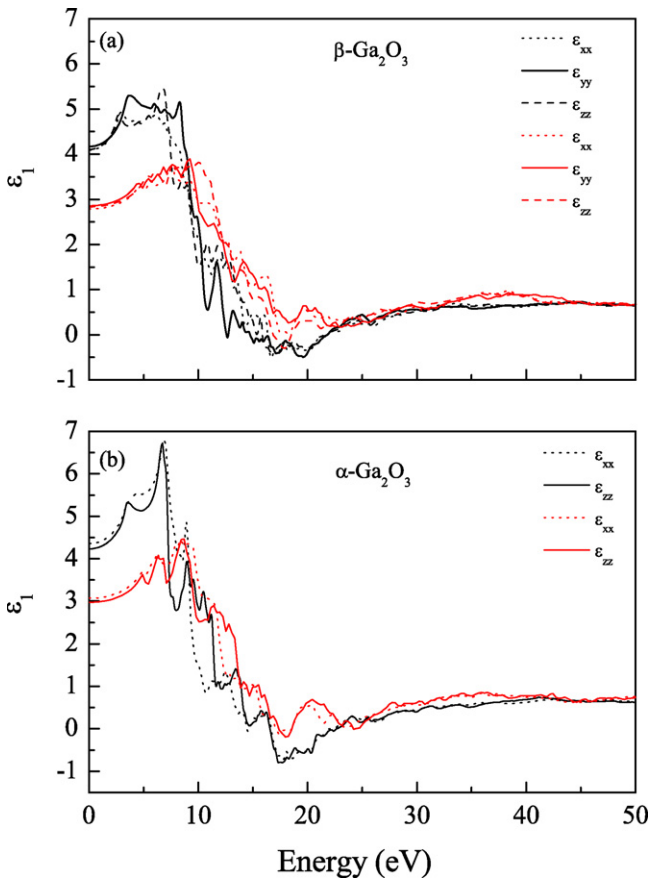

Fig. 7. Real part of dielectric function for (a) β-Ga_2O_3 and (b) α-Ga_2O_3. The B3LYP-DFT data (Ref. [25]) are plotted as a red line. ()

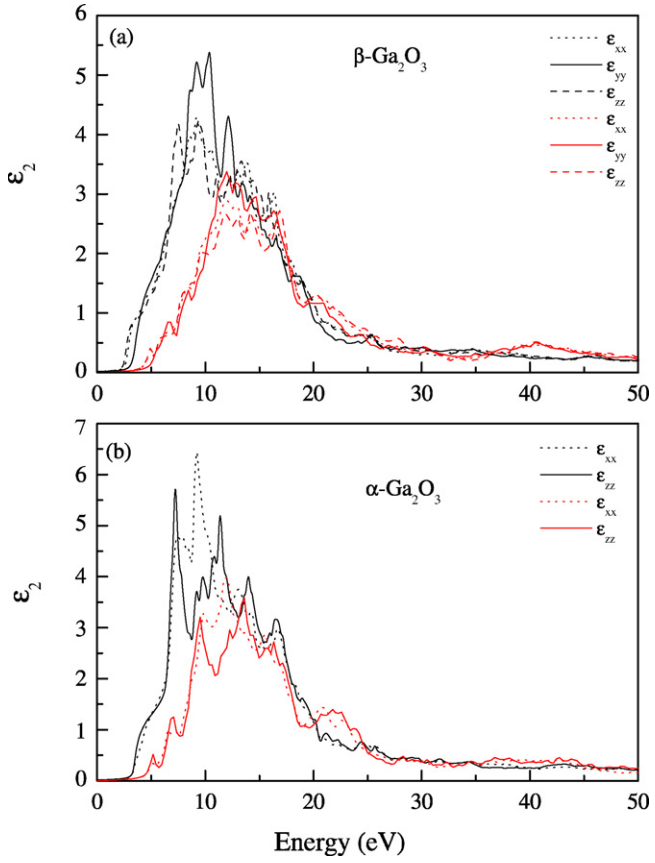

Fig. 8. Imaginary part of dielectric function for (a) β-Ga_2O_3 and (b) α-Ga_2O_3. The B3LYP-DFT data (Ref. [25]) are plotted as a red line. (For interpretation of the references to color in this figure legend, the reader is referred to the web version of the article.)

Table 4
Selected conduction and valence band eigenvalues measured from band structure calculation for the states close to the band edges at Γ of β and α phases of Ga_2O_3.

No.	E (eV)	
	β	α
58	5.723	6.722
57	2.362	3.031
56	−0.026	−0.265
55	−0.249	−0.265
54	−0.566	−0.306
53	−0.727	−0.319
52	−0.764	−0.319
51	−0.917	−0.530
50	−1.616	−0.530

in Figs. 7 and 8. He et al. results showed that the most pronounced peak was located at 12 eV which correspond to the value of 10.35/9.21 eV for β/α phases in our results. These peaks are related to the interband transition O 2p and Ga 4s. The smallest peak of Ref. [25] is found at 20 eV which correspond to the value 18.68/16.50 eV for β/α phases in our results. These later peaks correspond to the interband transition Ga 3d and Ga 4s. There are no clean-cut structures for $\varepsilon_2(\omega)$ above 26 eV, because the oscillator strengths coupling between the valance band (VB) and conduction band (CB) vanish. It is noted that a peak in $\varepsilon_2(\omega)$ does not correspond to a single interband transition since many direct or indirect transitions may be found in the band structure with an energy corresponding to the same peak.

The static dielectric constant $\varepsilon_1(0)$ is given by the low energy limit of $\varepsilon_1(\infty)$. Note that we do not include phonon contributions to the dielectric screening, and $\varepsilon_1(0)$ corresponds to the static optical dielectric constant $\varepsilon_1(\infty)$. Our calculated optical dielectric constants are listed in Table 5 along with the experimental and theoretical data. In view of Table 5, it is clearly seen, that our results are in good agreement with the available experimental and theoretical data when we take into account the correction of the band gap.

From the imaginary and the real parts of the dielectric function, we can calculate the other important optical function, including the refractive index $n(E)$ and the reflectivity $R(E)$. In Fig. 9 we present the refractive index $n(E)$ curves as a function of photon energy. The experimental results of real part $n(E)$ are reported by Passlacki et al. [13] using spectroscopic variable angle ellipsometry measurements and Rebien et al. [11] through the fitting of ellipsometry angles. Ortiz et al. [39] reported that the refractive index of Ga_2O_3 thin film deposited by periodic lattice-distortion (PLD) is about 1.85. We would like to mention that the quoted value (1.68) of the static dielectric constant (or refractive index n) of Ref. [25] is obtained by the Some Over States (SOS) method without relaxation.

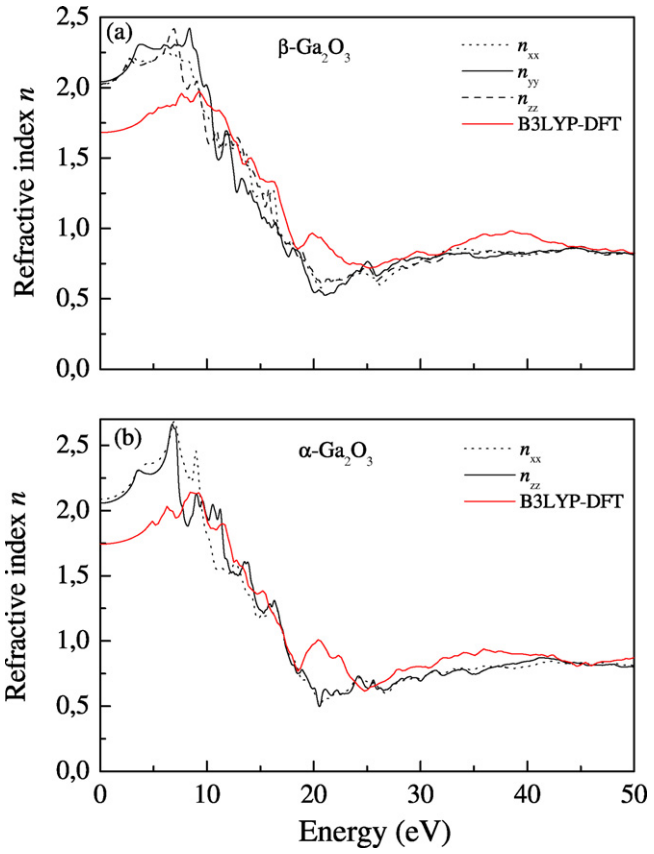

Fig. 9. Refractive index n of (a) β-Ga_2O_3 and (b) α-Ga_2O_3 as a function of photon energy. The B3LYP-DFT data (Ref. [25]) are plotted as a red line. (For interpretation of the references to color in this figure legend, the reader is referred to the web version of the article.)

This value is improved to (1.82) by using the Coupled-Perturbed Kohn–Sham (CPKS) or Finite Field (FF) method which takes into account the relaxation effects (the efficiency of this method can be seen in Refs. [25,51–53]). Our calculated results are consistent with the experimental values available in Table 5. The difference in the experimental values varies with the method of preparing thin films.

We have also presented the reflectivity spectra as a function of photon energy in Fig. 10. The small value of reflectance ensures its applications as transparent coatings in the visible to deep UV light regime. α-Ga_2O_3 shows an overall larger reflectance and a broader band in the range of 5–30 eV than β-Ga_2O_3. Our calculated results

Table 5
Optical dielectric constant, refractive index, and reflectivity of α-Ga_2O_3 and β-Ga_2O_3 compared to the theoretical calculations of Ref. [25]. The experimental values are also shown.

	β-Ga_2O_3				α-Ga_2O_3			
	Present[a]	Present[b]	Ref. [25]	Expt.	Present[a]	Present[c]	Ref. [25]	Expt.
ε_{xx}	4.094	3.475	2.78		4.36	3.867	3.07	
ε_{yy}	4.17	3.553	2.84		4.36	3.867	3.07	
ε_{zz}	4.11	3.481	2.86		4.23	3.76	2.97	
$\bar{\varepsilon}$	4.12	3.503	2.82	3.57[d], 3.38, 3.53[e]	4.30	3.813	3.03	3.69, 3.80[f]
$\bar{n}$	2.03	1.87	1.68	1.89[d], 1.84, 1.88[e]	2.07	1.95	1.74	1.92, 1.95[f]
$\bar{R}$	0.116	0.092	0.06		0.12	0.10	0.07	

[a] Without correction.
[b] With correction of the band gap $\Delta E_g = 2.238$ eV.
[c] With correction of the band gap $\Delta E_g = 1.628$ eV.
[d] Ref. [11].
[e] Ref. [13].
[f] Ref. [56].

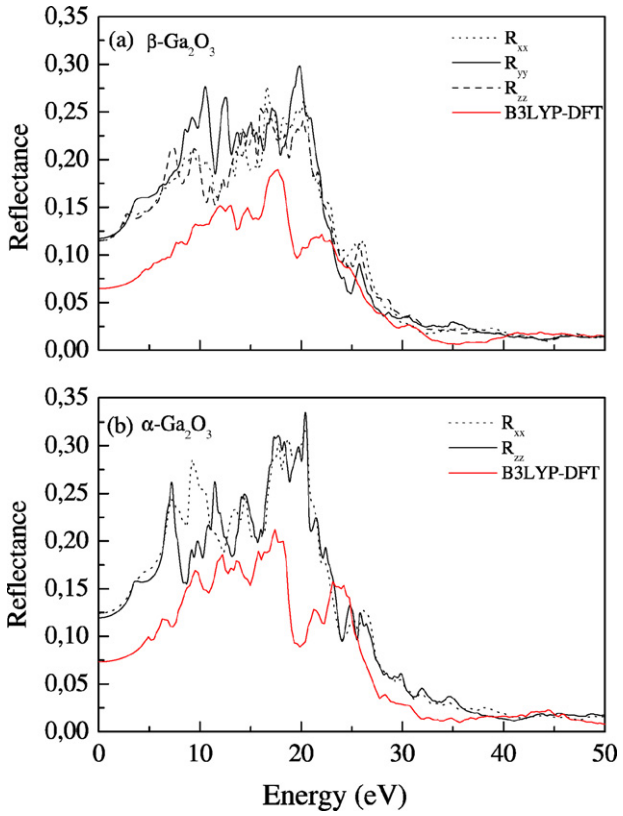

Fig. 10. The reflectivity R of (a) β-Ga_2O_3 and (b) α-Ga_2O_3 as a function of photon energy. The B3LYP-DFT data (Ref. [25]) are plotted as a red line. (For interpretation of the references to color in this figure legend, the reader is referred to the web version of the article.)

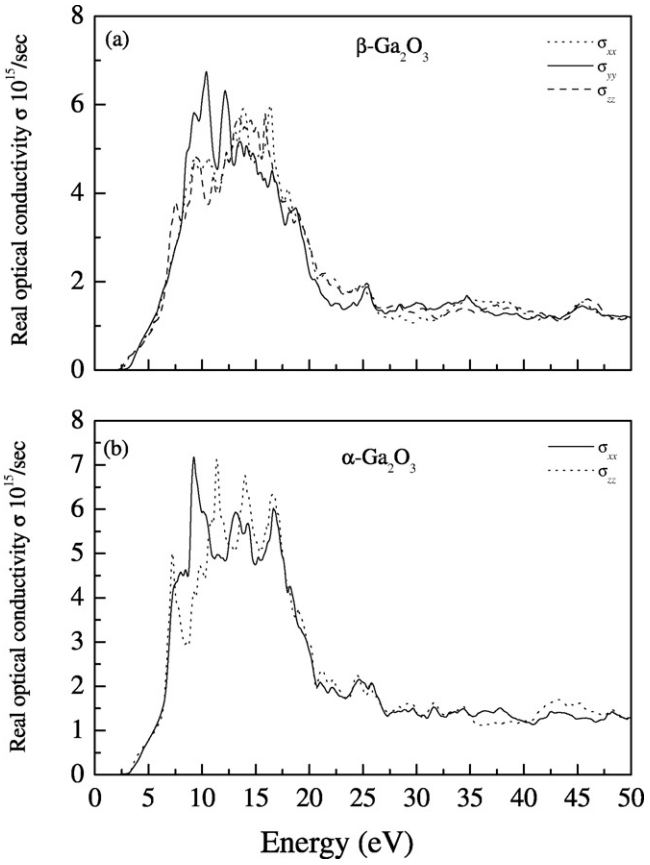

Fig. 11. Optical conductivity of (a) β-Ga_2O_3 and (b) α-Ga_2O_3.

show that the maximum reflectivity is at 19.8/20.42 eV, where the minimum reflectivity is at 25.72/25.78 eV in β/α.

The optical conductivity of β- and α-Ga_2O_3 in terms of energy was calculated and is shown in Fig. 11. The main peak around 10.38/9.21 eV in β/α phases was calculated. As we know from the literature, an exciton is a bound electron–hole pair, usually free to move together through the crystal. These excitons are produced when a photon of energy greater than the energy gap is absorbed in a crystal. These excitons may move through the crystal transporting energy but not charge. Because of its charge neutrality it does not contribute directly to the electrical conductivity. If an insulator contains bound electron–hole pairs it is called an excitonic insulator. However, it has been shown that Ga_2O_3 doping with Sn ions play a crucial role in realizing good conductivity [33]. In our case, from the optical conductivity we can see such excitonic features at 7.52/7.25, 10.38/9.21, 12.14/11.39, 13.89/14.0 and 16.36/16.64 eV in β/α phases.

EELS is a valuable tool for investigating various aspects of materials. It has the advantage of covering the complete energy range, including non-scattered and elastically scattered electrons (zero loss), which excite the electrons of the atom's outer shell (valence loss) or valence interband transitions. In Fig. 12 the energy loss function is plotted for β- and α-Ga_2O_3. The obtained spectrum of both structures are similar to that calculated by He and coworkers and to that of the experimental result [54]. The most prominent peaks *a*, *b*, *c*, and *d* in Fig. 12 are located at 13.9, 20.8, 22.7, and 29.3 eV in the experimental spectrum are shifted to *a*′, *b*′, *c*′, and *d*′ peaks located at 15.60/15.38, 23.03/23.30, 26.16/26.81, and 30.76/31.96 eV in β/α phases.

The energy of the main maximum is assigned to be the energy of the volume plasmon, $\hbar\omega_p$, and is equal to 26.16 and 26.81 eV for β- and α-Ga_2O_3, respectively. These later can be ascribed to the electron excitation from the O 2s level to the lower and upper conduction band. We note that the experimental spectrum was obtained for thin layers and temperature effects (vibration) may also become important in the experimental conditions. This explains the shift toward higher energy of the theoretical spectrum with respect to the experiment.

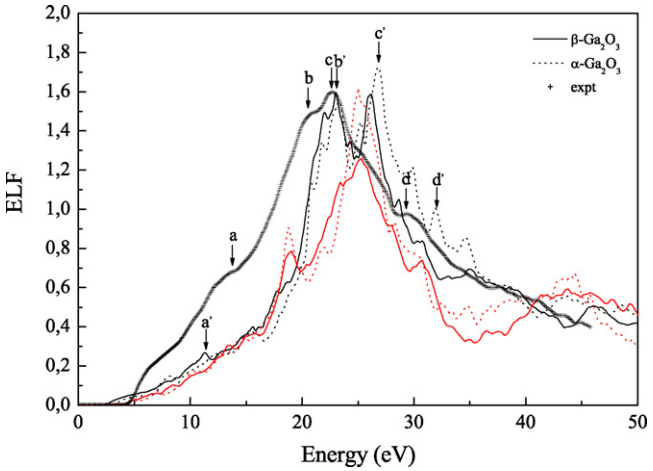

Fig. 12. Electron energy loss spectrum of β-Ga_2O_3 (full line) and α-Ga_2O_3 (doted line). The B3LYP-DFT data (Ref. [25]) are plotted as a red line. The experimental data taken from Schamm et al. [54] are plotted as plus signs and scaled to match the calculated peak maximum. (For interpretation of the references to color in this figure legend, the reader is referred to the web version of the article.)

4. Summary and conclusions

In summary, using the FPLAPW method, we have performed calculations on the structural, band structure and optical properties of β-Ga_2O_3 and α-Ga_2O_3. The total energy calculation for the ground-state structural properties of β and α phases shows excellent agreement with experimental data. The transition pressure at which this compound undergo the structural phase transition from β to α phase is found to be 9.28 GPa.

Several features of β-Ga_2O_3 resemble those of α-Ga_2O_3. Most of the calculated band parameters, including the energy band gaps, the total and the upper-valence bandwidths for α-Ga_2O_3 are close to those of β-Ga_2O_3 to within 1%. The charge distributions have similar features and shows strong ionic bonds, with charge localized at the Oxygen atoms, for both phases. The band-to-band transition can be identified from the critical points exhibited in the calculated dielectric function, which is consistent with the experimental results. The refractive index, extinction coefficient and reflectivity have also been calculated from obtained dielectric function, which are in agreement with the experimental results.

Acknowledgments

One of the authors (R. Khenata), express the sincere gratitude to Professors: Michel Rérat from Pau-University-France and Ravindra Pandey from Michigan Technological University-USA for their help.

References

[1] R. Roy, V.G. Hill, E.F. Obson, J. Am. Chem. Soc. 74 (1952) 719.
[2] A.C. Tas, P.J. Majweski, F. Aldinger, J. Am. Ceram. Soc. 85 (2002) 1421.
[3] G. Sinha, D. Ganguli, S. Chaudhuri, J. Phys.: Condens. Matter 18 (2006) 11167.
[4] H.H. Tippins, Phys. Rev. 140 (1965) A316.
[5] L. Binet, D. Gourier, J. Phys. Chem. Solids 59 (1998) 1241.
[6] J. Hao, M. Cocivera, J. Phys. D: Appl. Phys. 35 (2002) 433.
[7] N. Ueda, H. Hosono, R. Waseda, H. Kawazoe, Appl. Phys. Lett. 70 (1997) 3561.
[8] N. Ueda, H. Hosono, R. Waseda, H. Kawazoe, Appl. Phys. Lett. 71 (1997) 933.
[9] M. Ogita, N. Saika, Y. Nakanishi, Y. Hatanaka, Appl. Surf. Sci. 142 (1999) 188.
[10] R. Pohle, M. Fleischer, H. Meixner, Sens. Actuat. B 68 (2000) 151.
[11] M. Rebien, W. Herion, M. Hong, J.P. Mannaerts, M. Fleischer, Appl. Phys. Lett. 81 (2002) 250.
[12] F.K. Shan, G.X. Liu, W.J. Lee, G.H. Lee, I.S. Kim, B.C. Shin, J. Appl. Phys. 98 (2005) 023504.
[13] M. Passlacki, E.F. Schubert, W.S. Hobson, M. Hong, N. Moriya, S.N.G. Chu, K. Konstadinidis, J.P. Mannaerts, M.L. Schnoes, G.J. Zydzik, J. Appl. Phys. 77 (1995) 686.
[14] D.D. Edwards, T.O. Mason, F. Goutenoire, K.R. Poeppelmeier, Appl. Phys. Lett. 70 (1997) 1706.
[15] Z. Hajnal, J. Miró, G. Kiss, F. Réti, P. Deák, R.C. Herndon, J.M. Kuperberg, J. Appl. Phys. 86 (1999) 3792.
[16] E. Aubay, D. Gourier, Phys. Rev. B 47 (1993) 15023.
[17] R. Rao, A.M. Rao, B. Xu, J. Dong, S. Sharma, M.K. Sunkara, J. Appl. Phys. 98 (2005) 094312.
[18] H.W. Kim, N.H. Kim, J. Mater. Sci. 40 (2005) 4703.
[19] D. Machon, P.F. McMillan, B. Xu, J. Dong, Phys. Rev. B 73 (2006) 094125.
[20] G. Sinha, K. Adhikary, S. Chaudhuri, J. Cryst. Growth 276 (2005) 204.
[21] E.A. Albanesi, S.J. Sferco, I. Lefebvre, G. Allan, G. Hollinger, Phys. Rev. B 46 (1992) 13260.
[22] M.A. Blanco, M.B. Sahariah, H. Jiang, A. Costales, R. Pandey, Phys. Rev. B 72 (2005) 184103.
[23] K. Yamaguchi, Solid State Commun. 131 (2004) 739.
[24] H. He, M.A. Blanco, R. Pandey, Appl. Phys. Lett. 88 (2006) 261904.
[25] H. He, R. Orlando, M.A. Blanco, R. Pandey, E. Amzallag, I. Baraille, M. Rérat, Phys. Rev. B 74 (2006) 195123.
[26] S. Yoshioka, H. Hayashi, A. Kuwabara, F. Oba, K. Matsunaga, I. Tanaka, Condens. Matter 19 (2007) 346211.
[27] H. Kim, W. Kim, J. Appl. Phys. 62 (1987) 2000.
[28] P. Wu, Y.M. Gao, R. Kershaw, K. Dwight, A. Wold, Mater. Res. Bull. 25 (1990) 357.
[29] M. Passalack, E.F. Schubert, W.S. Hobson, M. Hong, N. Moriya, S.N.G. Chu, J. Appl. Phys. 77 (1995) 686.
[30] X. Wu, W. Song, W. Huang, M. Pu, B. Zhao, Y. Sun, J. Du, Chem. Phys. Lett. 328 (2000) 5.
[31] G. Park, W. Choi, J. Kim, Y. Choi, Y. Lee, C. Lim, J. Cryst. Growth 220 (2000) 494.
[32] W. Han, P. Kohler-Redlich, F. Ernst, M. Rühle, Solid State Commun. 115 (2000) 527.
[33] M. Orita, H. Ohta, M. Hirano, Appl. Phys. Lett. 77 (2000) 4166.
[34] Z.W. Pan, Z.R. Dai, Z.L. Wang, Science 291 (2001) 1947.
[35] C. Liang, G. Meng, G. Wang, Y. Wang, L. Zhang, S. Zhang, Appl. Phys. Lett. 78 (2001) 3202.
[36] J. Li, X. Chen, Z. Qiao, M. He, H. Li, J. Phys.: Condens. Matter 13 (2001) L937.
[37] M. Yamaga, M. Honda, Phys. Rev. B 68 (2003) 155207.
[38] N. Suzuki, S. Ohira, M. Tanaka, T. Sugawara, K. Nakajima, T. Shishido, Phys. Stat. Sol. (c) 4 (7) (2007) 2310.
[39] A. Ortiz, J.C. Alonso, E. Andrade, C. Urbiola, J. Electrochem. Soc. 148 (2001) F26.
[40] S. Geller, J. Chem. Phys. 33 (1960) 676.
[41] M. Marezio, J.P. Remeika, J. Chem. Phys. 46 (1967) 1862.
[42] P. Blaha, K. Schwarz, G. K. H. Madsen, D. Kvasnicka, J. Luitz, WIEN2k, An Augmented Plane Wave Plus Local Orbitals Program for Calculating Crystal Properties, Vienna University of Technology, Vienna, Austria, 2001.
[43] P. Hohenberg, W. Kohn, Phys. Rev. 136 (1964) B864.
[44] W. Kohn, L.J. Sham, Phys. Rev. 140 (1965) A1133.
[45] E. Sjostedt, L. Nordstrom, D.J. Singh, Solid State Commun. 114 (2000) 15.
[46] G.K.H. Madsen, P. Blaha, K. Schwarz, E. Sjostedt, L. Nordstrom, Phys. Rev. B 64 (2001) 195134.
[47] K. Schwarz, P. Blaha, G.K.H. Madsen, Comput. Phys. Commun. 147 (2002) 71.
[48] J.P. Perdew, Y. Wang, Phys. Rev. B 45 (1992) 13244.
[49] F.D. Murnaghan, Proc. Natl. Acad. Sci. U.S.A. 30 (1944) 5390.
[50] J.P. Remeika, M. Marezio, J. Am. Chem. Soc. 8 (1966) 87.
[51] C. Darrigan, M. Rérat, G. Mallia, R. Dovesi, J. Comput. Chem. 24 (2003) 1305.
[52] M. Rérat, R. Dovesi, in: T. Simos, G. Maroulis (Eds.), International Conference of Computational Methods in Sciences and Engineering (ICCMSE 2004), Lecture Series on Computer and Computational Sciences, vol. 1, Brill Academic, Leiden, The Netherlands, 2004, p. 771.
[53] M. Ferrero, M. Rérat, R. Orlando, R. Dovesi, J. Chem. Phys. 128 (2008) 014110.
[54] S. Schamm, G. Zanchi, Ultramicroscopy 96 (2003) 559.
[55] G. Schmitz, P. Gassmann, R. Franchy, J. Appl. Phys. 83 (1998) 2533.
[56] R.C. Weast (Ed.), CRC Handbook of Chemistry and Physics, 70th ed., CRC, Boca Raton, 1989, p. B-92.